Computational fluid dynamics in the upper airway: comparison between different models and experimental data for a simplified geometry with major obstruction

Fatemeh Entezari Heravi, Mohammad Ali Nazari, Franz Chouly, Pascal Perrier, Yohan Payan

Computational fluid dynamics in the upper airway: comparison between different models and experimental data for a simplified geometry with major obstruction

Fatemeh Entezari Heravi[1], Mohammad Ali Nazari[1], Franz Chouly[2], Pascal Perrier[3] and Yohan Payan[4]

[1]School of Mechanical Engineering, College of Engineering, University of Tehran, Tehran, Iran
[2]Laboratoire de Mathématiques de Besançon, UBFC, F-25000 Besançon cedex, France
[3]Univ. Grenoble Alpes & CNRS, Gipsa-lab, F-38000 Grenoble, France
[4]Univ. Grenoble Alpes & CNRS, TIMC-IMAG,F-38000 Grenoble, France

Abstract

The present study aims at comparing different computational models used for simulating the fluid-structure interaction within an in-vitro setup resembling simplified major obstruction of pharyngeal airway. Due to the nature of the problem, i.e. air flow passing over a deformable latex surface, a fully coupled fluid-structure interaction algorithm is used. A comparison is made between two finite element models for the solid domain, one using shell and the other using volume elements. The material properties of these models follow a hyperelastic behavior. For the fluid part, laminar and various turbulence models such as standard $k-\varepsilon$, Shear Stress Transport, SSG Reynolds Stress and BSL Reynolds Stress are compared. We evaluate the efficiency of the models and how close to the experimental data are their results. The predictions of the structural model containing volume elements showed better consistency with the experimental data. In addition, the results obtained with the standard $k-\varepsilon$ turbulence model were the least deviated among all turbulence models.

Keywords: Fully coupled fluid-structure interaction; pharyngeal airway; finite element method; laminar fluid flow; turbulent fluid flow.

1 Introduction

Numerical modelling of flows in human body is of great importance. Various studies have been focusing on the airflow along the respiratory system, particularly in the upper airway. Some of them have modeled only fluid flow assuming rigid boundaries. For instance, Wang et al. (2009) [1] have predicted the airflow along the upper airway during a whole respiratory cycle using $k-\varepsilon$ turbulence model for the transient analysis. In Mylavarapu et al. (2009) [2], various turbulence models such as unsteady Large Eddy Simulation (LES) model and some of the steady Reynolds-Averaged Navier-Stokes (RANS) models, i.e. $k-\varepsilon$, $k-\omega$, $k-\omega$-based Shear Stress Transport, and Spallart-Alarmas models, are compared on the basis of flow computation in the upper airway. In the aforementioned study, the peak expiratory flow rate goes through the upper airway and the regions of minimum negative pressure are determined. These regions are those where the obstruction is most likely to occur. The characteristics of the flow pattern in the inspiratory phase are discussed in Sung et al. (2006) [3] and the regions prone for obstruction in nasal cavity and in the pharynx are determined using RNG $k-\varepsilon$ model, which is a

modified version of the standard $k-\varepsilon$ model that takes account of the contribution of different turbulence scales rather than considering only the length scale. The Spalart-Allmaras model is preferred by Nithiarasu et al. (2008) [4] and they claim that this model is commonplace for incompressible flow calculations. Their study resulted in specifying the regions of minimum negative pressure by studying the steady inspiratory flow. In Lucey et al. (2010) [5], the Shear Stress Transport Turbulence (SST) model is employed to predict the airflow pattern during the inhalation phase of the respiratory cycle within a 3D pharyngeal geometry reconstructed from the data of optical coherence tomography (OCT) which could capture multi-sectional images of a tissue structure (Fujimoto (2000) [6]). Moreover, in this study, the effect of different wall positions is taken into account through a change of the initial rigid wall geometry. Based on a brief comparison of the results of laminar flow model, $k-\varepsilon$ model, and $k-\omega$ SST turbulence model they concluded that the SST model would be more appropriate than the other three. The response of the upper airway to the mandibular advancement splint in treating major obstructions of the airway is investigated in Zhao et al. (2013) [7]. In this study, the $k-\omega$ based Shear Stress Transport model is considered appropriate for the upper airway flow. The effect of nasal obstruction in positive airway pressure treatment therapy is studied using Spalart-Allmaras model in Wakayama et al. (2016) [8]. In Cisonni et al. (2013) [9] the pressure drop in the velopharynx of subjects with and without obstructions in the upper airway was computed using fluid flow simulations with $k-\omega$ SST modeling on the anatomies constructed from optical coherence tomography (OCT).

The effect of fluid pressure on deformable parts of the upper airway has been studied in Pelteret and Reddy (2014) [10] and Carrigy et al. 2015 [11]. In Pelteret and Reddy (2014) [10] the fluid pressure changes sinusoidally to represent the effect of inhaling and exhaling but its magnitude is considered uniform except in the mouth region where it decreases linearly from the tip of tongue to the pharyngeal part of the tongue to model the inhaling through the mouth. The simulation is then completed using FEM analysis. In Carrigy et al. (2015) [11] a uniform negative pressure is applied on the whole model to study the effect of area changes in velar and oral parts. Then the aforementioned authors determined the most appropriate Young's Moduli of the muscles and the adipose tissues assuming a linear elastic model.

In other studies the assumption of rigid boundaries has been replaced by a more realistic one. There are several works where both the airflow and its deformable pathway are modeled using fluid-structure interaction (FSI) method. In Huang et al. (2008) [12] a two-dimensional finite-element model of the upper airway is examined under laminar flow conditions taking into account the muscle's active properties. A 2D FSI simulation is carried out upon a simplified geometry for both normal and abnormal pharyngeal airways in Wang et al. (2009) [1]. In Chouly et al. (2008) [13] the FSI method is used for coupling a 3D deformable solid model and a 2D fluid model of the expiratory flow in the upper airway during major obstructions. In this study, flow features are analyzed with Reduced Navier-Stokes/Prandtl (RNS/P) equations which are described in Lagrée and Lorthois (2005) [14]. These equations are also used for the analysis of the flow in a 2D model of the oropharynx in Chouly et al. (2006) [15]. A 3D model of the expiratory airflow is simulated with fully coupled FSI method in Rasani et al. (2011) [16]. $k-\omega$ based Shear Stress Transport model is adopted for this study. In Heil (2003) [17], a review is published that presents numerous models used for investigating general characteristics of airflow in interaction with soft tissues throughout the human body. These models range from zero-equation models to three-dimensional Navier-Stokes simulations. This publication emphasizes the necessity and importance of fully-coupled approaches for dealing with such problem. Such a fully coupled FSI simulation is used by

Wang et al. (2012) [18] for determining the efficiency of nasal surgery, where the standard $k-\omega$ turbulence model is employed for simulating the flow domain. The same is done by Zhao et al. (2013) [19] for the study on mandibular advancement method, using the $k-\omega$ based Shear Stress Transport. The deformation along the entire upper airway is studied by transient flow analysis coupled with linear structural analysis in Kim et al. (2015) [20] using Large Eddy Simulation model for the transient analysis of the fluid domain. In Pirnar et al. (2015) [21] both soft palate flutter and the airway narrowing are simulated through fully coupled FSI method. In all of these fluid-structure interaction studies, the solid domain is considered linearly elastic.

Given the diversity of the models available for simulating fluid-structure interaction in the upper airways, and the variety of their predictions in the context of the study of the sleep apnea syndrome~~,~~ a precise and quantitative assessment of these different approaches is needed. In this aim, we propose to take the measures carried out by Chouly et al. (2008) with a replica of the pharyngeal airway as reliable reference data to which the predictions of the models will be precisely and quantitatively compared. The advantage of using these experimental results is that they were obtained in controlled conditions through precise measurement techniques which could not be achieved while working with patient-specific data. In order for increasing the accuracy of the results, a fully coupled method is chosen as the fluid-structure coupling algorithm, and hyperelastic material properties are assigned to the solid domain. In previous works Chouly et al. (2008) [13] using RNS/P equations provided predictions of the pressure drop within the constriction of the pharyngeal replica, and of the flow-induced deformation, that fitted well the experimental data. Nevertheless, in order to go further and carry out later on simulations from real and complex patient-specific geometries, other fluid flow models should be considered. Indeed RNS/P equations are mostly limited to simple 2D geometries and induce numerical difficulties in case of heavy recirculation after the constriction. Therefore, complete 3D Navier-Stokes equations with laminar or turbulent closures should be considered, as they are now available in standard finite element packages such as ANSYS/FLUENT(TM). In addition, since various turbulent models are provided in ANSYS/CFX 15.0 and are used in biomedical simulations, their predictive performance and accuracy for studying such a complex phenomenon need to be compared using relevant experimental data. The efficiencies of two different finite element models for the solid domain are examined; one containing shell elements and, the other, volume elements. Some of the most commonplace flow models, i.e. laminar, standard $k-\varepsilon$, Shear Stress Transport, and BSL and SSG Reynolds Stress models, are compared to each other in this study ("BSL" and "SSG" stand for "Baseline" and "Speziale, Sarkar, Gatski" respectively). The pressure value at the point where the constriction is the narrowest is used as a key variable for comparing the results of the numerical models and the experimental results reported in Chouly et al. (2008) [22].

2 Theoretical assumptions and materials

2.1 Governing Equations

For appropriate simulations of fluid-structure interaction problems such as highly deformable tissues interacting with turbulent flows, an iterative fully coupled transient algorithm is suggested where fluid and solid equations are solved by separate solvers. Especially having large deformations in solid domain would affect the boundary conditions of the fluid flow. In this algorithm, two constraints are set at the interface of the fluid and solid domains for coupling. The first constraint is the relationship between the displacement in the solid domain and the fluid velocity at each interface node as:

$$\mathbf{u} = \frac{\partial \mathbf{d}}{\partial t} \tag{1}$$

where $\mathbf{u}$ is the fluid velocity vector and $\mathbf{d}$ is the displacement vector of the structure.

The second coupling constraint is the equivalence of the Cauchy stress tensors of the two domains as,

$$\boldsymbol{\sigma}^f \mathbf{n}^f + \boldsymbol{\sigma}^s \mathbf{n}^s = 0 \tag{2}$$

where $\mathbf{n}^s$ and $\mathbf{n}^f$ are the outward unit normal vectors on the solid and fluid surfaces at their interface, $\boldsymbol{\sigma}^f$ and $\boldsymbol{\sigma}^s$ are the Cauchy stress tensors of the fluid and solid domains respectively. Cauchy stress tensor in solid follows a neo-Hookean hyperelastic constitutive law:

$$\boldsymbol{\sigma}^s = \frac{C_1}{J^{5/3}}(\mathbf{B} - \frac{1}{3} tr(\mathbf{B})\mathbf{I}) + K(J-1)\mathbf{I} \tag{3}$$

where **I** is the unit second order stress tensor, **B** is the left Cauchy-Green strain tensor, and C_1, and K are shear modulus, and bulk modulus respectively. J is the Jacobian of deformation and is equal to $\sqrt{\det(\mathbf{B})}$. This formulation of the stress is derived from the strain energy function for the nearly incompressible isotropic neo-Hookean hyperelastic material defined in Nazari et al. (2010) [23] as:

$$W = \frac{C_1}{2}\left(J^{-2/3} I_1 - 3\right) + \frac{K}{2}(J-1)^2 \tag{4}$$

where $I_1 = tr(\mathbf{B})$ is the first invariant of the Cauchy-Green strain tensor.

The Cauchy stress tensor in the Stokes fluid flow is:

$$\boldsymbol{\sigma}^f = -p\mathbf{I} + 2\mu(\mathbf{V} - \frac{1}{3} tr(\mathbf{V})\mathbf{I}) \tag{5}$$

where $\mathbf{V}$ is the strain rate tensor and p is the fluid pressure. $\mathbf{V}$ is defined as:

$$\mathbf{V} = \frac{1}{2}(\nabla \mathbf{u} + \nabla \mathbf{u}^{\mathbf{T}}) \tag{6}$$

where $\mathbf{u}$ stands for the fluid velocity, and ∇ is gradient.

The general characteristics of the flow are considered to be Newtonian, inviscid, and incompressible. Therefore the incompressible Navier-Stokes equations are,

$$\boldsymbol{\nabla} \cdot \mathbf{u} = 0 \tag{7}$$

$$\rho(\mathbf{u} \cdot \boldsymbol{\nabla})\mathbf{u} = -\boldsymbol{\nabla} P + \boldsymbol{\nabla}(2\mu \mathbf{V}) \tag{8}$$

where $\mathbf{u}$ is the fluid velocity, ρ is the fluid density, μ is the dynamic viscosity, and $\mathbf{V}$ is the strain rate tensor.

For turbulent flows, the velocity vector and pressure are considered as the sum of a mean ($\mathbf{U}, P$), and a fluctuating part ($\mathbf{u}', p'$)**:**

$$\mathbf{u} = \mathbf{U} + \mathbf{u}' \tag{9 a}$$

$$p=P+p' \tag{9 b}$$

With Reynolds time averaging defined as,

$$\bar{\mathbf{f}} = \lim_{\mathrm{T}\to\infty} \frac{1}{T}\int_{t}^{t+T} \mathbf{f}(s)\, ds \tag{10}$$

and by applying this type of averaging on Eq. (7) and Eq. (8) using Eqs. (9), the Reynolds averaged equation of mass conservation, and the Reynolds Averaged Navier-Stokes (RANS), are derived as:

$$\boldsymbol{\nabla} \cdot \mathbf{U} = 0 \tag{11}$$

$$\rho(\mathbf{U} \cdot \boldsymbol{\nabla})\mathbf{U} = -\boldsymbol{\nabla} P + \boldsymbol{\nabla}[2\mu\mathbf{V} - \rho\boldsymbol{\tau}] \tag{12}$$

where $\rho\boldsymbol{\tau}$ is called Reynolds Stress tensor. The components of this tensor are equal to $\rho\overline{\mathbf{u}'\otimes\mathbf{u}'}$ ($\otimes$ stands for the dyadic product of two vectors) and the way one defines it determines the type of the flow model with which the simulation is to be done (Wilcox(1993) [24]). For laminar flow, this term would be zero, because the velocity field is assumed to have no fluctuation in any direction. In turbulence modeling, there are two major ways for defining this term. In the first way, the Eddy Viscosity model assumes that Reynolds stresses are proportional to mean velocity gradients and are defined as:

$$\rho\overline{\mathbf{u}'\otimes\mathbf{u}'} = \mu_t\mathbf{V} - \frac{2}{3}\mathbf{I}(\rho k) \tag{13}$$

where k is the turbulence kinetic energy defined as $k = \frac{\overline{\mathbf{u}'\cdot\mathbf{u}'}}{\mathbf{2}}$, and μ_t is the eddy viscosity or turbulent viscosity; in the $k-\varepsilon$ model and the Shear Stress Transport Model μ_t is respectively defined as:

$$\mu_t = C_\mu \rho \frac{k^2}{\varepsilon} \tag{14}$$

$$\mu_t = \rho \frac{\alpha k}{\max(\alpha\omega, SF)} \tag{15}$$

where C_μ and α are constant parameters, ε is the turbulence eddy dissipation rate, ω is the specific dissipation rate, S is an invariant of the strain rate matrix, and F is a blending function. These variables are defined trough the following equations:

$$\varepsilon = \nu\overline{\boldsymbol{\nabla}\mathbf{u}' : \boldsymbol{\nabla}\mathbf{u}'} \tag{16}$$

$$\omega = \frac{\varepsilon}{k} \tag{17}$$

$$F = \tanh(f^2) \tag{18}$$

where f is defined as,

$$f = \max\left(\frac{2\sqrt{k}}{\beta\omega y}, \frac{500\nu}{y^2\omega}\right) \tag{19}$$

where ":" shows double contraction of two second-order tensors, β is a constant, y is the distance to the nearest wall, and ν is the kinematic viscosity.

The second common way for modeling Reynlods Stress Tensor term is called Reynolds Stress model. It is based on solving transport equations for all Reynolds stress tensor components and the dissipation rate. Two of the most commonplace methods of this type are SSG Reynolds Stress model and BSL Reynolds Stress model whose formulations could be found in Eisfeld (2010) [25].

The simulation is conducted through three levels of iteration, (a) the field loop, used to converge toward a solution for each field with the associated solver, (b) the coupling loop, used for exchanging loads or displacements between the two fields, and, (c) the time loop which intends to make each step move forward in time. Within each field loop, the governing equations of the flow, Eq. (7) and Eq. (8), are solved for finding the value of pressure and velocity vector at nodes. During the coupling (stagger) loop, the results of the fluid field solver are applied to the relevant nodes of the solid domain using Eq. (2). The solid field solver computes the deformation of the structure and the results are applied on the fluid interface with solid domain as a new set of boundary conditions during the coupling loop using Eq. (1). This iterative coupling procedure continues until the convergence tolerance or the maximum number of iterations is reached. For a steady-state FSI simulation the solution for fluid domain is quasi-static and for solid domain is transient within each field loop (Gianopapa, 2004 [26]).

2.2 Material properties

We have seen above that the solid domain is considered to follow the neo-Hookean material model. Solid domain is of latex material and its elastic parameters are $E = 1.68$ MPa and $\nu = 0.499$ (Chouly et al., 2008).

Linearization of Eq. (4) at initial point gives,

$$C_1 = E/3 \tag{20}$$

And with the assumption of nearly incompressible material the material constants are given in Table 1.

Table 1 Constants of the neo-Hookean $\boldsymbol{W}$ function

$C_1\ (Pa)$	$K/2\ (1/Pa)$
560000	$7.1429e-09$

The fluid material is set as air at 25°C with $\rho = 1.185\,\frac{kg}{m^3}$ and $\mu = 1.831 \times 10^{-5}\,\frac{kg}{ms}$.

3 Finite Element Model

The geometry of the pharyngeal replica setup was created using the dimensions reported in Chouly et al. (2008) (Fig. 1). The model is build up in ANSYS release 15. Fig. 2 represents the finite element model of the latex surface. The mesh in Fig. 2(a) consists of a layer of 8-node quadrilateral SHELL181 elements, and the one in Fig. 2(b) consists of 20-node hexahedral SOLID186 elements along with 10-node SOLID 187 elements. The SOLID187 elements are distributed through the thickness and they count to 337 out of 1760 total elements. The number of elements and nodes of these two models are given in Table 2. The thickness of latex layer is $0.3\ mm$. As shown, the latex surface is divided into two regions. The core region is in interaction with the airflow and the surrounding region is attached to the rigid pipe. Water

flows in this pipe to apply a constant pressure against the core region. In order to simulate the conditions of the experimental setup an external pressure of $300\ \mathrm{Pa}$ is applied on the upper surface of the core region and its inferior surface is supposed to act as the interface of the fluid and structure domains. The nodes of the surrounding region are fixed. The total time for simulation is considered to be 1s. The solution time step size is set as a function of inlet pressure to overcome convergence issues. It varies between 1e-5 to 1e-3 second.

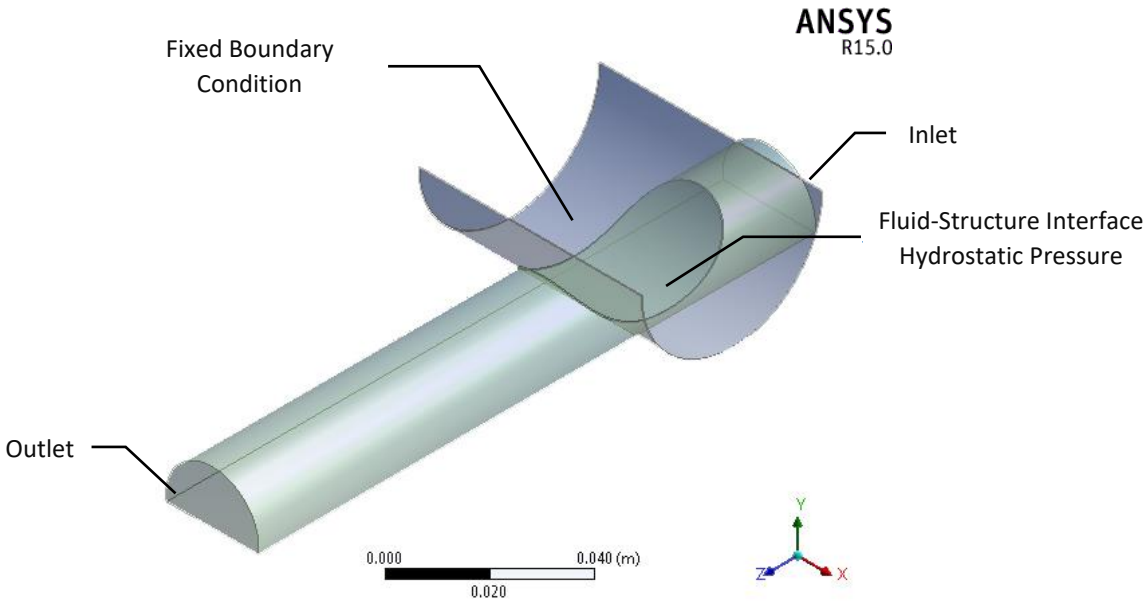

Figure 1 Geometry of the pharyngeal replica setup

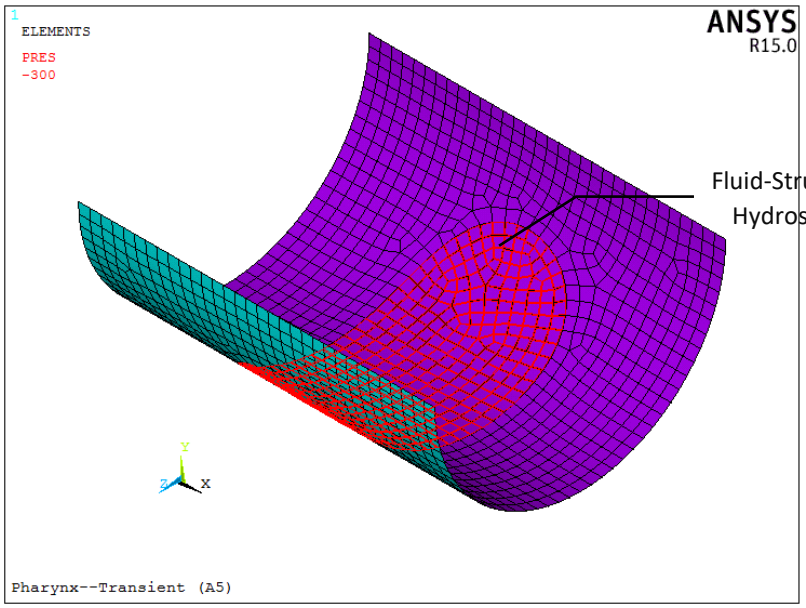

(a)

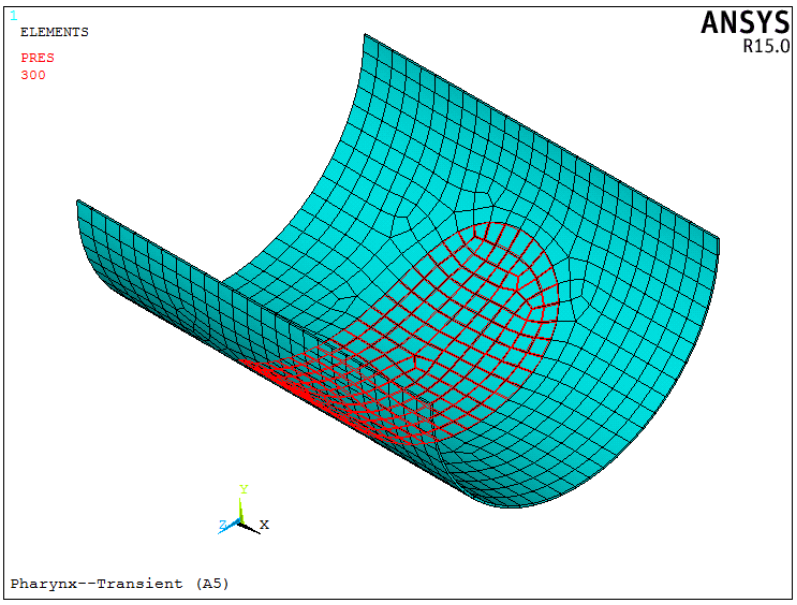

(b)

Figure 2 FEM model of the latex surface. (a) Model containing two-dimensional shell elements. (b) Three dimensional model.

Table 2 Number of nodes of the solid models

2D Shell Model	3D Model
3239	7819

The finite element model of the setup airway is depicted in Fig. 3.

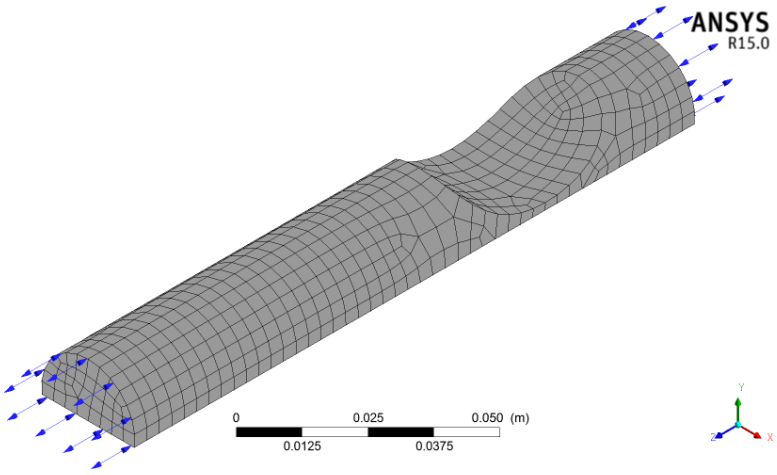

Figure 3 Finite element model of the simplified pharyngeal airway

Fluid mesh consists of 2082 nodes in 2216 finite volume elements from which 1222 are hexahedral. The reason for using this relatively coarse mesh is to avoid using a mesh that captures the fine scales in the fluid in the turbulent models such as $k-\varepsilon$ method. Indeed such fine scales generate turbulent vortices that unrealistically dissipate in the solution yielding an inaccurate simulation. The inlet total

pressure, P_i, ranges from 100 Pa to 600 Pa and the outlet static pressure is considered to be 0 Pa. All pressure values are taken with respect to atmosphere. The walls of the airway are rigid except the section interacting with the solid domain.

4 Results

4.1 Influence of the mesh used for the solid domain

The pressure at the constriction, P_c, is used as a basis for comparison between the experimental setup and the model. Fig. 4 illustrates a comparison of P_c resulting from using either shell or volume elements to model the solid domain. These results are also presented in Table 3. The flow model was considered to be $k-\varepsilon$ in this case.

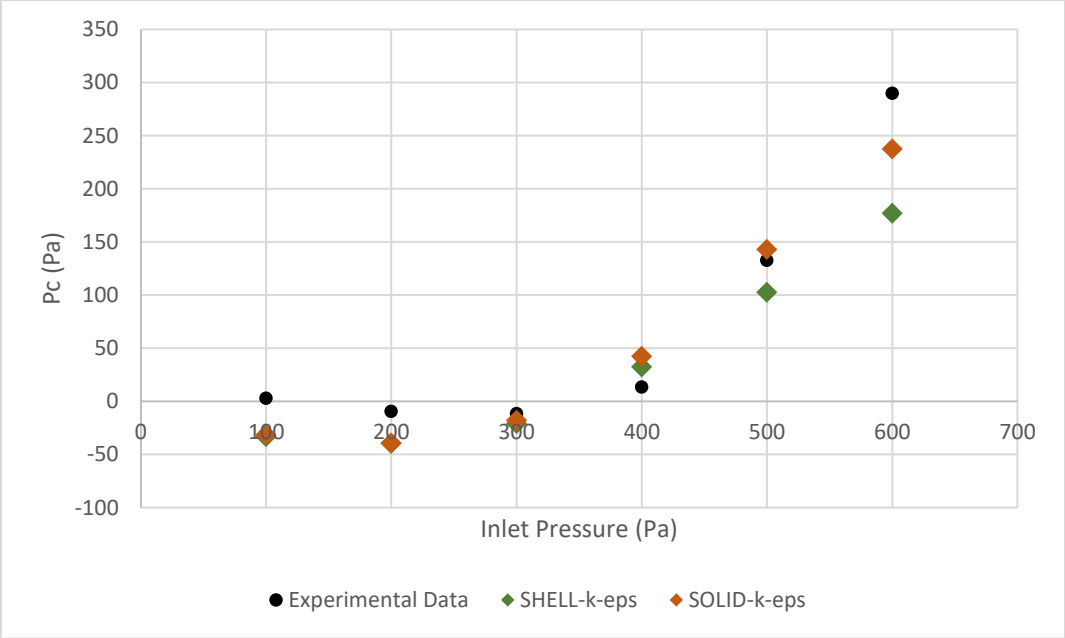

Figure 4. Comparison of the results of shell and volume elements

Table 3 Comparison of the results of shell and volume elements

	P_c (Pa)		
Inlet pressure (Pa)	Experimental Data	Shell elements, $k-\varepsilon$	Volume elements, $k-\varepsilon$
100	3.2	-33.0	-31.2
200	-9.1	-39.3	-38.9
300	-11.2	-20.8	-17.6
400	13.6	32.5	42.7
500	133	102.7	143.0
600	290	177.2	237.7

The coefficient of determination, R^2, was computed as 0.92 for the model with volume elements, and 0.78 for that with shell elements. Comparing these values, we observed a trend for the volume element to work better for simulating such thin hyper-elastic surfaces interacting with the passage of fluid flow.

4.2 Influence of the flow model

In Fig. 5, the value of P_c is indicated vs. different values of inlet pressure using each one of the flow models described in section 2.1. The three-dimensional structure is chosen for the solid domain in this comparison. The results are also presented in Table 4.

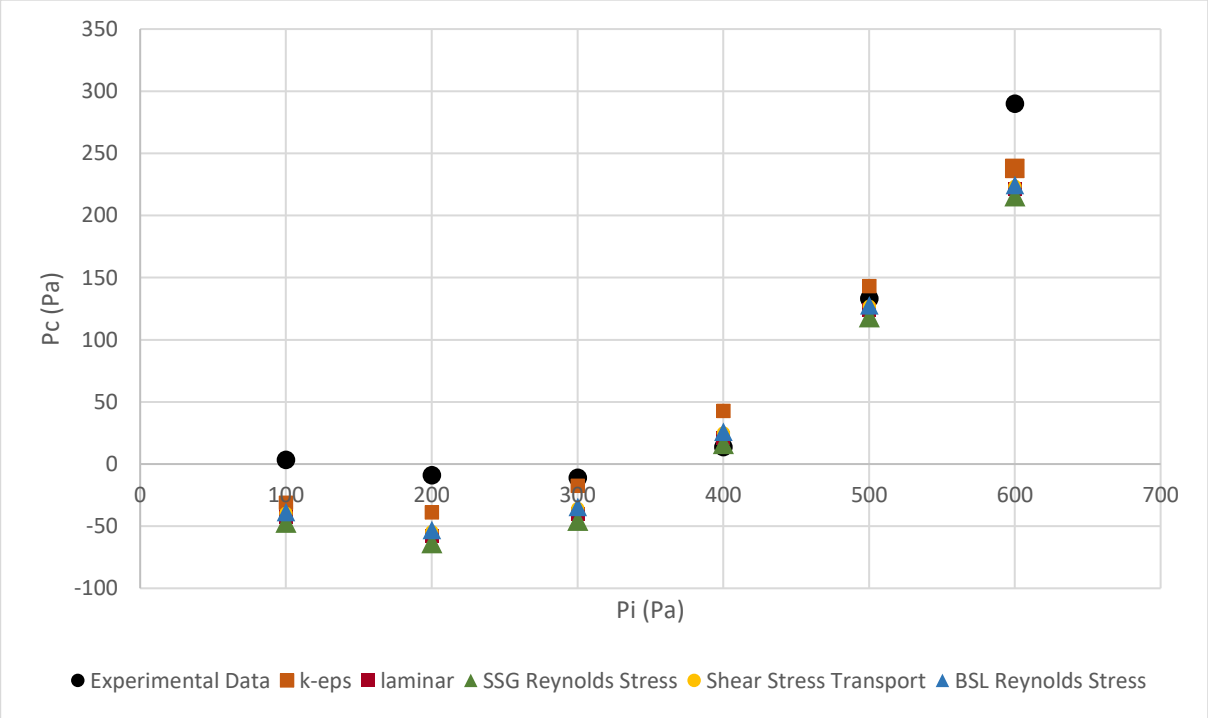

Figure 5 Comparison of the results of different fluid models. The solid domain was modeled with volume elements.

Table 4 Comparison of the results of different fluid models. The solid domain was modeled with volume elements.

	P_c (Pa)					
Inlet pressure (Pa)	Experimental Data	$k-\varepsilon$	Laminar	SSG Reynolds Stress	Shear Stress Transport	BSL Reynolds Stress
100	3.2	-31.2	-42.6	-47.0	-39.7	-38.7
200	-9.1	-38.9	-57.6	-63.3	-54.3	-53.0
300	-11.2	-17.6	-40.0	-45.3	-35.8	-34.6
400	13.6	42.7	21.0	16.4	25.0	26.0
500	133	143.0	123.5	118.3	126.8	127.7

600	290	237.7	220.8	215.8	223.3	224.5

The R^2 parameter is calculated for these models and is given in Table 3. As can be seen in Fig. 5, and according to the value of R^2 for each case, the standard $k-\varepsilon$ model seems to be slightly better than other approaches for modeling the fluid. However, it should be noticed that by using the laminar model, the simulations would be less complicated due to the elimination of time-dependent fluctuating turbulent parameters. In addition, the coefficient of determination in Chouly et al. (2008) [22] is computed as 0.58 for an applied external pressure of 300 Pa. Comparing the results obtained from solving a 2D flow model in Chouly et al. (2008) [22] with those reported in Table 5, the necessity of 3D simulation for modeling the fluid-structure interaction problems is justified.

Table 5 R^2 parameters calculated for the different flow models interacting with the 3D solid mesh

Laminar	$k-\varepsilon$	Shear Stress Transport	SSG Reynolds Stress	BSL Reynolds Stress
0.86	0.92	0.88	0.84	0.88

The contour of deformation for the interface is shown in Fig. 6. This contour is the result of a 400 Pa inlet pressure set for the simulation with volume elements and $k-\varepsilon$ flow model. The flow streamlines are also illustrated in Fig. 7. The streamline pattern before and after the constriction region justifies the asymmetric deformation of the pharyngeal part of the tongue. Maximum deformation has occurred after the constriction zone where the negative pressure over the surface is maximum. Therefore, the probable occlusion has the highest chance to occur after the initial stenosis region.

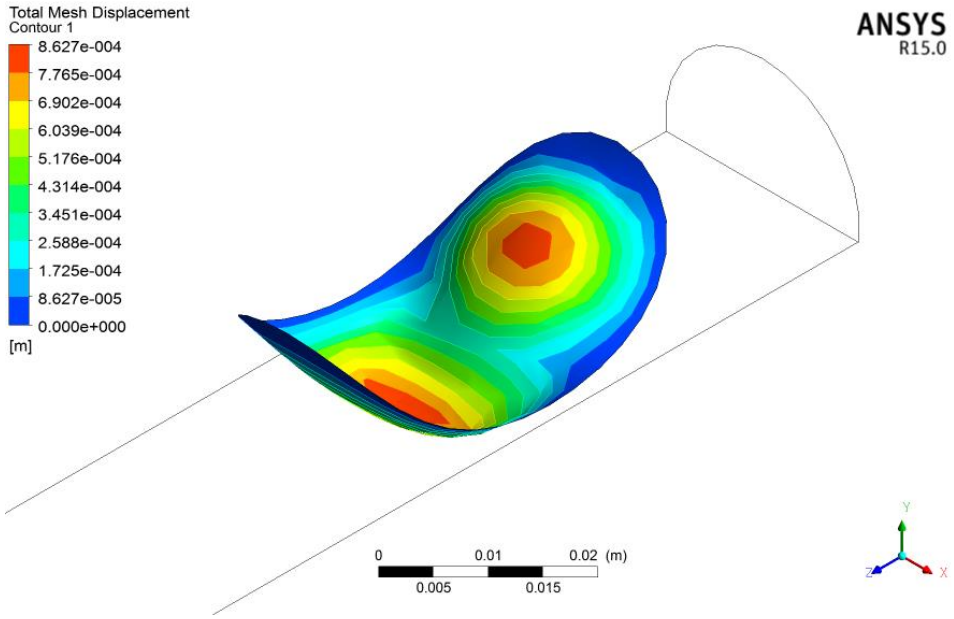

Figure 6 Deformation of latex surface (in meter) for $P_i = 400$ Pa (displacements scaled for better visualization)

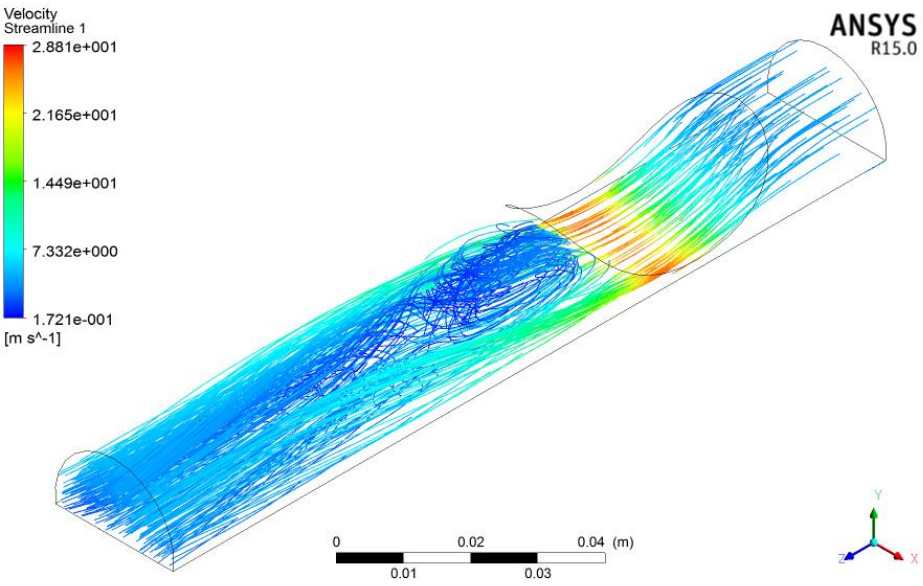

Figure 7 The flow streamlines for $P_i = 400$ Pa

5 Conclusion

The goal of this study was to assess the accuracy of various 3D flow models in predicting the airflow properties of the pharyngeal airway in the case of major obstruction-using a fully coupled fluid-structure interaction method. To this purpose, we relied on precise and quantitative experimental data coming from an in-vitro replica of the pharyngeal airway [13].The solid material was assumed to be an isotropic, incompressible neo-Hookean hyperelastic one. The performances of shell and 3D finite element were compared with each other in the solid domain. Also, for the fluid domain, a comparison was made between laminar flow model and four Reynolds-Averaged Navier-Stokes (RANS) models, namely the standard $k-\varepsilon$, the $k-\omega$ based Shear Stress Transport, the BSL Reynolds Stress, and the SSG Reynolds Stress model. The pressure at the constriction point was obtained from all numerical models and was compared with the experimental data. Nearly all of the models provided correct results. Among these, the results of standard $k-\varepsilon$ flow model fitted best; however, the accuracy of laminar model results was reasonable and this model could be used in order for avoiding difficulties associated with tuning parameters in turbulence modeling. Both volume and shell elements worked well; though it could be seen that volume elements give slightly better results for modeling the solid. This finding is consistent with the results published in (Landajuela et al. (2016) [27]).

The result of this work could be further applied on the realistic human oropharyngeal model for the study and analysis of the Syndrome of Obstructive Sleep Apnea (OSA). A transient study could be done for simulating the respiratory cycles for both normal and patient cases. Also, possible treatments could be simulated before they are examined on a patient in order to reduce possible side effects and risk factors.

Acknowledgement

This work has been supported by Center for International Scientific Studies and Collaboration (CISSC) and French Embassy in Tehran in the framework of the project Hubert Curien Gundishapur BIOSTOC.

References

[1] Wang, Y., Liu, Y.., Sun, X., Yu, S., Gao, F., 2009. Numerical analysis of respiratory flow patterns within human upper airway. Acta Mechanica Solida Sinica 25:737-746.

[2] Mylavarapu, G., Murugappan, S., Mihaescu, M., Kalra, M., Khosla, S., Gutmark, E., 2009. Validation of computational fluid dynamics methodology used for human upper airway flow simulations. Journal of Biomechanics 42:1553-1559.

[3] Sung, S.J., Jeong, S. J., Yu, S. Y., Hwang, C. J., Pae, E. K., 2006. Customized three-dimensional Computational fluid dynamics simulation of the upper airway of obstructive sleep apnea. Angle Orthodontist 76 (5):791-9.

[4] Nithiarasu, P., Hassan, O., Morgan, K., Weatherill, N. P., Fielder, C., Whittet, H., Ebden, P., Lewis, K. R., 2008. Steady flow through a realistic human upper airway geometry. International Journal For Numerical Methods In Fluids 57:631-651

[5] Lucey, A. D., King, A. J. C., Tetlow, G. A., Wang, J., Armstrong, J. J., Leigh, M. S., Paduch, A., Walsh, J. H., Sampson, D. D., Eastwood, P.R., Hillman, D. R., 2010. Measurement, reconstruction, and flow-field computation of the human pharynx with application to sleep apnea. IEEE Transactions on Biomedical Engineering 57(10):2535-2548.

[6] Fujimoto, J. C., Pitris, C., Boppart, S. A., Brezinski, M. E., 2000. Optical Coherence Tomography: An emerging technology for biomedical imaging and optical biopsy. Neoplasia 2:9-25.

[7] Zhao, M., Barber, T., Cistulli, P. A., Sutherland, K., Rosengarten, G., 2013. Computational fluid dynamics for the assessment of upper airway response to oral apliance treatment in obstructive sleep apnea. Journal of Biomechanics 46:142-150.

[8] Wakayama, T., Suzuki, M., Tanuma, T., 2016. Effect of nasal obstruction on continuous positive airway pressure treatment: Computational Fluid Dynamics Analyses. PLOS ONE 11(3).

[9] Cisonni, J., Lucey, A. D., Walsh, J. H., King, A. J. C., Elliott, N. S.J., Sampson, D. D., Eastwood, P.R., Hillman, D. R., 2013. Effect of the velopharynx on intraluminal pressures in reconstructed pharynges derived from individuals with and without sleep apnea. Journal of Biomechanics 46(14):2504-2512.

[10] Pelteret, J.-P. V., Reddy, B., 2014. Development of a computational biomechanical model of the human upper airway soft tissues toward simulating obstructive sleep apnea. Clinical Anatomy 27:182-200.

[11] Carrigy, N. B., Carey, J. P., Martin, A. R., Remmers, J. E., Zaerian, A., Topor, Z., Grosse, Z., Noga, M., Finlay, W. H., 2015. Simulation of muscle and adipose tissue deformation in the passive human pharynx. Computer Methods in Biomechanics and Biomedical Engineering 19(7): 1025-5842.

[12] Huang, Y., Malhotra, A., White, D. P., 2005. Computational simulation of human upper airway collapse using a pressure-/state-dependent model of genioglossal muscle contraction under laminar flow conditions. Journal of Applied Physiology 99:1138-1148.

[13] Chouly, F., Van Hirtum, A., Lagree, P.-Y., Pelorson, X., Payan, Y., 2008. Numerical and experimental study of expiratory flow in the case of major obstructions with fluid-structure interaction. Journal of Fluids and Structures 24:250-269.

[14] Lagrée, P. Y., Lorthois, S. (2005). The RNS/Prandtl equations and their link with other asymptotic descriptions: application to the wall shear stress scaling in a constricted pipe. International Journal of Engineering Science 43(3), 352-378.

[15] Chouly, F., Van Hirtum, A., Lagrée, P. Y., Paoli, J. R., Pelorson, X., & Payan, Y., 2006, Simulation of the retroglossal fluid-structure interaction during obstructive sleep apnea. Lecture Notes in Computer Science 4072.

[16] Rasani, M. R., Inthavong, K., Tu, J. Y., 2011. Simulation of pharyngeal airway interaction with airflow using low-Re turbulence model. Modeling and Simulation in Engineering 510472.

[17] Heil, M., Jensen, O. E., 2003. Flows in deformable tubes and channels. In Flow past highly compliant boundaries and in collapsible tubes, Springer Netherlands: 15-49.

[18] Wang, Y., Wang, J., Liu, Y., Yu, S., Sun, X., Li, S., Shen, S., Zhao, W. 2012. Fluid–structure interaction modeling of upper airways before and after nasal surgery for obstructive sleep apnea. International Journal For Numerical Methods In Biomedical Engineering, 28(5), 528-546.

[19] Zhao, M., Barber, T., Cistulli, P. A., Sutherland, K., Rosengarten, G., 2013. Simulation of upper airway occlusion without and with mandibular advancement in obstructive sleep apnea. Journal of Biomechanics 46: 2586-2592.

[20] Kim, S.-H., Chung, S.-K., Na, Y., 2015. Numerical investigation of flow-induced deformation along the human respiratory upper airway. Journal of Mechanical Science and Technology 29(12): 5267-5272.

[21] Pirnar,J., Dolenc-Groselji, L., Fajdija, I., Zun, I., 2015. Computational fluid-structure interaction simulation of flow in the human upper airway. Journal of Biomechanics 48: 3685-3691.

[22] Chouly, F., Van Hirtum, A., Lagree, P.-Y., Perloson, X., Payan, Y., 2008. Modelling human pharyngeal airway: validation of numerical simulations using in vitro experiments. Medical and Biological Engineering and Computing 47: 49-58.

[23] Nazari, M. A., Perrier, P. , Chabanas, M. , Payan, Y., 2010. Simulation of dynamic orofacial movements using a constitutive law varying with muscle activation. Computer Methods in Biomechanics and Biomedical Engineering 13(4): 469-489.

[24] Wilcox, D. C., 1993. Turbulence Modeling for CFD. Glendale, California: DCW Industries, Inc.

[25] Eisfeld, B., 2010. Reynolds stress modelling for complex aerodynamic flows. In European Conference on Computational Fluid Dynamics, ECCOMAS CFD: 14-17.

[26] Gianopapa, C. G., 2004. Fluid-structure interaction in flexible vessels. PhD thesis, University of London, King's College London.

[27] Landajuela, M., Vidrascu, M., Chapelle, D., Fernandez, M. A., 2016. Coupling schemes for FSI forward prediction challenge: comparative study and validation. International Journal for Numerical Methods in Biomedical Engineering. In press. DOI:10.1002/cnm.2813.